Pergamon

Int. J. Heat Mass Transfer. Vol. 39, No. 7, pp. 1331–1342, 1996

0017-9310/96 $15.00 + 0.00

0017-9310(95)00234-0

Mixed convection in a vertical parallel-plate channel partially filled with porous media of high permeability

WEN-JENG CHANG and WEN-LUNG CHANG

Department of Mechanical Engineering, Feng Chia University, Taichung, Taiwan, Republic of China

(*Received* 9 *December* 1994 *and in final form* 23 *June* 1995)

Abstract—The purpose of the present study is to analyze numerically the developing mixed convection in a vertical parallel-plate channel partially filled with porous medium. The SIMPLEC algorithm combining the techniques of ADI and SOR is used in this study. The diffusion and convection are handled by a hybrid scheme. The non-Darcy model, which includes inertia effect, boundary friction effect and convection, is used in the momentum equations for the porous medium layer. The velocity and temperature distributions, local Nusselt number (Nu_x), local friction coefficient (C_f), pressure drop and entrance length in a vertical parallel-plate channel partially filled with porous medium are obtained under various parameters, such as different thickness of porous medium (Rs), Darcy number (Da), Grashof number (Gr). The numerical results of this investigation show that (a) the local Nusselt number increases as Rs decreases and Da and Gr increase; (b) the local friction coefficient increases as Da and Gr increase; and (c) the pressure drop in the parallel-plate channel increases as Rs increases and Da decreases. There is a minimum non-zero local friction coefficient where the thickness of the porous medium is about 0.2. Hydrodynamic entrance length is shorter as the value of Rs is increased, and is longer as the values of Da and Gr are increased. Thermal entrance becomes longer as the values of Rs and Da increase and shorter as the values of Gr increase.

1. INTRODUCTION

Using the porous medium and fluid layers (also called composite system), the heat transfer and flow field of two parallel plates with many tightly arrayed fins in the heat exchangers can be simulated. A similar condition can be found in a large computer cabinet where there are many integrated circuits on the main board that are similar to a porous layer. When cooling air flows through channels between main boards, the case can be assumed that fluid flows through a channel with a fluid layer having a porous layer on each side.

The convection will be influenced by the interaction of the flow and porous medium on the permeable interface of the composite system. In order to realize the change of heat transfer, flow field, friction drag of fluid when flowing through the parallel-plate channel with fins, and the channel between main boards with integrated circuits, we conducted a basic research for the convective phenomena by using a vertical parallel-plate channel partially filled with porous medium.

There have been some investigations of the porous/fluid composite system on natural convection, but there have been very few researches conducted on forced convection in recent years. Prasad [1] has made an excellent review for composite systems. Poulikakos *et al.* [2] studied the convection for composite system consisting of a fluid layer and packed bed heated from below. Schulenberg and Muller [3] also studied natural convection in a saturated porous layer with internal heat sources and an adiabatic boundary on the lower side. Poulikakos [4] discussed the thermal instability in a horizontal fluid layer superposed on a heat generating porous bed. Taslim and Narusawa [5] performed the thermal instability in a composite system in which a porous layer is sandwiched between two fluid layers. Sathe *et al.* [6] researched natural convection in a rectangular cavity with porous/fluid layers and permeable interface. Beckermann *et al.* [7, 8] also made a deep analysis of heat transfer with various positions allocated for porous/fluid layers. Campos *et al.* [9] studied the natural convection of an enclosed cylinder partially filled with porous medium while heated inside and cooled outside.

For the forced convection of a composite system, this study will briefly introduce the related papers separated into internal and external flow fields. For the external flow field, as far as authors known, there have been few investigations about external forced convection fluid flow and heat transfer in the composite system. Vafai and Kim [10] have studied the forced convection over an external boundary lined with a porous substrate. They found that the porous substrate significantly reduces frictional drag at the wall. Huang and Vafai [11] analyzed changes in flow pattern and heat transfer characteristics due to the existence of the multiple porous block structure and compared the results with ref. [10].

For the internal flow field, an empirical approach using the Darcy theorem for tangential velocity at the

NOMENCLATURE

C	inertia coefficient
C_f	friction coefficient
C_p	specific heat
Da	Darcy number, K/x_0^2
d_b	diameter of porous particle
Gama	ratio of porous medium and fluid conductivity (k_p/k_f)
Gr	Grashof number
h	heat transfer coefficient
K	permeability
k	thermal conductivity
Nu_x	local Nusselt number, $2hx_0/ke$
P_f	pressure of fluid
P_p	pressure in porous layer
P	dimensionless pressure in porous layer
Pr	effective Prandtl number in porous layer
Re	Reynolds number
Rs	dimensionless porous layer thickness, s/x_0
s	porous layer thickness
T_m	bulk mean temperature of both fluid and porous layers
T_0	inlet temperature of fluid
T_w	wall temperature
U	dimensionless horizontal velocity in porous layer, V_{xp}/V_0
V	dimensionless vertical velocity in porous layer, V_{yp}/V_0
V_0	inlet velocity of fluid
V_{xf}	horizontal velocity in fluid layer
V_{xp}	horizontal velocity in porous layer
V_{yf}	vertical velocity in fluid layer
V_{yp}	vertical velocity in porous layer
x	horizontal coordinate
x_0	half of the channel spacing
X	dimensionless horizontal coordinate, x/x_0
y	vertical coordinate
y_0	length of channel
Y	dimensionless vertical direction, y/x_0
Y_0	dimensionless length of channel, $Y_0 = 66$.

Greek symbols

α	diffusion coefficient $[k/(\rho C_p)]$
β	coefficient of volume expansion
ρ	density
μ	dynamic viscosity
ν	kinematic viscosity ($\nu = \mu/\rho$)
θ	dimensionless temperature in porous layer, $\theta = (T_p - T_0)/(T_w - T_0)$
θ_b	dimensionless temperature in porous layer, $\theta_b = (T_p - T_0)/(T_m - T_0)$
θ_m	dimensionless temperature, $\theta_m = (T_m - T_0)/(T_w - T_0)$
θ_w	dimensionless wall temperature, $\theta_w = 1$
ε	porosity.

Superscript

*	fluid layer.

Subscript

e	effective
f	fluid
p	porous
w	wall
x	horizontal direction
y	vertical direction.

interface between a Newtonian fluid and an isotropic porous medium was first suggested by Beavers and Joseph [12] in 1967. Neale and Nader [13] repeated the research by using the Darcy–Brinkman model in 1974. They found the B–J slip condition is exactly satisfied. An excellent review of the research on flow past porous layers has been reported by Rudraiah [14]. Using the non-Darcy model, Poulikakos and Kazmierczal [15] and Jang and Chen [16] studied fully developed forced convection in a horizontal channel filled with porous/fluid layers. Vafai and Kim [17] developed an analytic solution for the fully developed composite system. Tong and Scharatchandra [18] also discussed the problem in ref. [17]. As far as we know, there are very few papers on the problems of mixed convection of developing or fully developed flow and heat transfer in a parallel-plate channel partially filled with porous medium. This has motivated the present investigation.

2. MATHEMATICAL FORMULATION

The analysis is based on solving the transport equations for two-dimensional flow through a vertical parallel-plate channel partially filled with porous medium, depicted in Fig. 1. The two parallel plates have an equal and constant temperature (T_w) on the wall. Fluid enters the parallel-plate channel from below with a uniform velocity profile (V_0) and a constant low temperature (T_0). The symbol, Rs, represents the dimensionless thickness of porous layer. It is assumed that the flow is steady, laminar, two-dimensional and incompressible. The radiation and thermal dissipation effect are neglected. In addition, permeability and thermal conductivity of porous medium are homogeneous and isotropic, and in local thermal equilibrium with the fluid. The Boussinesq's approximation is valid, and $\rho = \rho_w[1 - \beta(T - T_w)]$ for fluid density is adopted in the buoyancy term. There

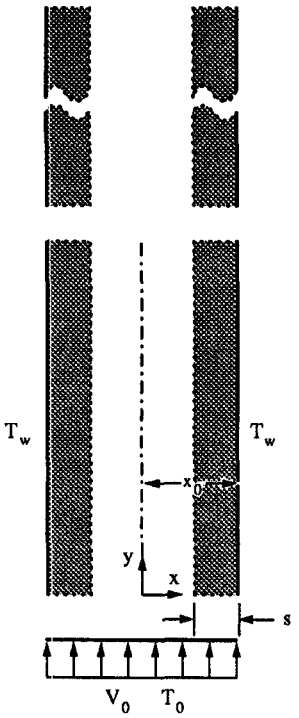

Fig. 1. Physical model and coordinate system of vertical parallel-plate channel.

is no heat source and chemical reaction in the parallel-plate channel.

The conservation equations for mass, momentum, energy, and boundary conditions in the fluid region are

$$\frac{\partial U^*}{\partial X}+\frac{\partial V^*}{\partial Y}=0 \tag{1}$$

$$U^*\frac{\partial U^*}{\partial X}+V^*\frac{\partial U^*}{\partial Y}=-\frac{\partial P^*}{\partial X}+\frac{1}{Re^*}\left(\frac{\partial^2 U^*}{\partial X^2}+\frac{\partial^2 U^*}{\partial Y^2}\right) \tag{2}$$

$$U^*\frac{\partial V^*}{\partial X}+V^*\frac{\partial V^*}{\partial Y}=-\frac{\partial P^*}{\partial Y}+\frac{1}{Re^*}\left(\frac{\partial^2 V^*}{\partial X^2}+\frac{\partial^2 V^*}{\partial Y^2}\right)+\frac{Gr^*}{Re^{*2}}(\theta^*-1) \tag{3}$$

$$U^*\frac{\partial \theta^*}{\partial X}+V^*\frac{\partial \theta^*}{\partial Y}=\frac{1}{Pr^*Re^*}\left(\frac{\partial^2 \theta^*}{\partial X^2}+\frac{\partial^2 \theta^*}{\partial Y^2}\right) \tag{4}$$

$$X=0 \quad U^*=0 \quad \frac{\partial V^*}{\partial X}=0 \quad \frac{\partial \theta^*}{\partial X}=0$$

$$Y=0 \quad U^*=0 \quad V^*=1 \quad \theta^*=0$$

$$Y=Y_0=\frac{y_0}{x_0} \quad U^*=0 \quad \frac{\partial V^*}{\partial Y}=0 \quad \frac{\partial \theta_b^*}{\partial Y}=0. \tag{5}$$

All the variables in the fluid region have been non-dimensionalized based on the following definitions:

$$X=\frac{x}{x_0} \quad Y=\frac{y}{x_0} \quad U^*=\frac{V_{xf}}{V_0} \quad V^*=\frac{V_{yf}}{V_0}$$

$$P^*=\frac{P_f}{\rho V_0^2} \quad Pr^*=\frac{\nu_f}{\alpha_f} \quad \theta^*=\frac{T_f-T_0}{T_w-T_0} \quad \theta_b^*=\frac{T_f-T_0}{T_m-T_0}$$

$$Gr^*=\frac{g\beta(T_w-T_0)x_0^3}{\nu_f^2} \quad Re^*=\frac{V_0\cdot x_0}{\nu_f}, \tag{6}$$

where T_m is the bulk mean temperature of both fluid and porous layers.

The generalized flow model known as the Brinkman–Forchheimer-extended Darcy model was used in the conservation equations in the porous region. The following are the governing equations in the porous region:

$$\frac{\partial U}{\partial X}+\frac{\partial V}{\partial Y}=0 \tag{7}$$

$$U\frac{\partial U}{\partial X}+V\frac{\partial U}{\partial Y}=-\varepsilon^2\frac{\partial P}{\partial X}+\frac{\varepsilon}{Re}\left(\frac{\partial^2 U}{\partial X^2}+\frac{\partial^2 U}{\partial Y^2}\right)-\varepsilon^2\left(\frac{1}{DaRe}+\frac{C}{\sqrt{Da}}|\bar{V}|\right)U \tag{8}$$

$$U\frac{\partial V}{\partial X}+V\frac{\partial V}{\partial Y}=-\varepsilon^2\frac{\partial P}{\partial Y}+\frac{\varepsilon}{Re}\left(\frac{\partial^2 V}{\partial X^2}+\frac{\partial^2 V}{\partial Y^2}\right)-\varepsilon^2\left(\frac{1}{DaRe}+\frac{C}{\sqrt{Da}}|\bar{V}|\right)V+\varepsilon^2\frac{Gr}{Re^2}(\theta-1) \tag{9}$$

$$U\frac{\partial \theta}{\partial X}+V\frac{\partial \theta}{\partial Y}=\frac{1}{PrRe}\left(\frac{\partial^2 \theta}{\partial X^2}+\frac{\partial^2 \theta}{\partial Y^2}\right). \tag{10}$$

K and C are the permeability and inertia coefficients of porous medium and are represented, respectively, by the correlations [19]:

$$K=\frac{d_b^2\varepsilon^3}{175(1-\varepsilon)^2} \quad C=\frac{1.75}{\sqrt{175}}\varepsilon^{-1.5}$$

$$X=1 \quad U=0 \quad V=0 \quad \theta=1$$

$$Y=0 \quad U=0 \quad V=1 \quad \theta=0$$

$$Y=Y_0=\frac{y_0}{x_0} \quad U=0 \quad \frac{\partial V}{\partial Y}=0 \quad \frac{\partial \theta_b}{\partial Y}=0. \tag{11}$$

All the variables in the porous region also have been nondimensionalized based on the following definitions:

$$X=\frac{x}{x_0} \quad Y=\frac{y}{x_0} \quad U=\frac{V_{xp}}{V_0} \quad V=\frac{V_{yp}}{V_0}$$

$$P=\frac{P_p}{\rho V_0^2} \quad Pr=\frac{\nu_e}{\alpha_e} \quad \theta=\frac{T_p-T_0}{T_w-T_0} \quad \theta_b=\frac{T_p-T_0}{T_m-T_0}$$

$$Gr=\frac{g\beta(T_w-T_0)x_0^3}{\nu_e^2} \quad Re=\frac{V_0x_0}{\nu_e} \quad Da=\frac{K}{x_0^2}. \tag{12}$$

It should be noted that the relationships for Pr, Re and Gr in the fluid/porous layer are described as follows:

(1) Using the equation $k_e = \varepsilon k_f + (1-\varepsilon)k_p$ [20]. Where k_e is the effective thermal conductivity of the fluid-saturated porous layer, k_f and k_p are the thermal conductivity of the fluid and porous medium, respectively. So, we can have

$$Pr = Pr^*/[\varepsilon + (1-\varepsilon)\text{Gama}], \quad \text{where Gama} = \frac{k_p}{k_f}$$

(2) $v_e = v_f$ [13] then $Re = Re^*$ and $Gr = Gr^*$.

It is worthwhile to note that the interface of the composite system is handled as in Vafai and Kim [10] [using equations (1)–(4) and (7)–(10) to calculate the variables at the interface].

The local friction coefficient and local Nusselt number at the wall are

$$C_f = \frac{2}{Re}\frac{\partial V}{\partial X}\bigg|_{x=1} \quad \text{and} \quad Nu_x = \frac{2}{1-\theta_m}\frac{\partial \theta}{\partial X}\bigg|_{x=1},$$

$$\text{where } \theta_m = \frac{T_m - T_0}{T_w - T_0}.$$

3. NUMERICAL ANALYSIS

The model equations are solved numerically using the SIMPLEC algorithm. This approach was suggested by Doormaal and Raithby [21] who modified the SIMPLE algorithm initiated by Patankar and Spalding [22] and Patankar [23]. The hybrid scheme is used for the convection terms and diffusion terms. By using the idea of ref. [10], the set of differences is solved over the entire region of interest to obtain new values for any desired variable by taking into account the latest known estimated values of those variables on the neighboring nodes.

A numerical scheme with nonuniform 33×90 grids was applied to the present physical system. The finest grid, of size 0.01 and located adjacent to the wall, inlet region and interface of porous/fluid layer, is chosen to get more detailed situation of the flow field. The adequacy of the grid is verified by comparing the results computed with 60×90 grids and 60×142 grids. The comparisons for the temperature and velocity distributions at different directions are satisfied. The maximum discrepancy of local Nusselt numbers along surface is less than 5%. In order to diminish the memory and computational time and still have the numerical accuracy, the nonuniform 33×90 grids were applied to the present physical system.

Applying the discretization procedure, the coefficient matrix of difference equations is transformed into a tridiagonal matrix by the ADI scheme, and solved by the TDMA method. Meanwhile, we quoted the E-factor [21] and SOR scheme to increase the convergence speed in every iteration. The numerical iteration was repeated until the following convergence criterion was satisfied:

$$\max\left|\frac{\Phi_{i,j}^{n+1} - \Phi_{i,j}^{n}}{\Phi_{i,j}^{n}}\right| \leqslant 10^{-5},$$

where Φ could be the U, V, P, θ, U^*, V^*, P^* or θ^*.

4. RESULTS AND DISCUSSIONS

In order to confirm the validity of this numerical model, the numerical result was compared with the classical one in an extreme condition ($Rs = 0$, no porous medium). The obtained velocity, temperature, and local Nusselt number are in fairly good agreement with the data reported by Bejan [20], as shown in Table 1. In this study, the ranges of simulation parameters are: $0 \leqslant Rs \leqslant 0.5$, $10^{-5} \leqslant Da \leqslant 10^{-1}$, $0 \leqslant Gr \leqslant 10^4$, $Re = 50$, $Pr = 0.72$, $\varepsilon = 0.8$ and Gama $= 10$.

4.1. *Effects of porous layer thickness*

Figure 2 shows the effects of porous layer thickness on the flow velocity distribution in a vertical composite parallel-plate channel. Due to flow resistance in a porous medium, more fluid flows into the fluid layer from the porous layer as the thickness increases from 0 to 0.5. As a consequence, flow velocity near the center line of the parallel-plate channel increases as the thickness (Rs) increases. However, the hydrodynamic entrance length decreases as thickness (Rs) increases. The numerical results are also shown in Table 2. Figure 3 shows the variation of temperature distribution with different porous layer thicknesses. When the porous layer exists, i.e. $Rs > 0$ and $Y = 0.1$, there is a lower fluid temperature for $X > 0.74$ and $Rs = 0.5$. This is resulted by a large flow velocity in the porous layer. Because of high temperature fluid flowing into the fluid region and a high conductivity of porous medium, the fluid temperature is higher for $X < 0.74$ and $Rs = 0.5$. At $Y = 0.5$, the fluid temperature increases as the porous layer thickness increases. This is due to the high thermal conductivity of porous medium. When Y increases, the average flow velocity in the fluid layer decreases as the porous layer thickness decreases. More thermal energy is absorbed by fluid and the fluid temperature rises quickly. This results that the thermal entrance length becomes shorter as the porous layer thickness decreases. The numerical results are shown in Table 2.

Figure 4 shows the variation of the local Nusselt number with different porous layer thicknesses. For

Table 1. The comparison of present result of fully developed Nusselt number and Bejan's result [20]

Grids	Present result	Bejan result [20]
33×90	7.543	7.54

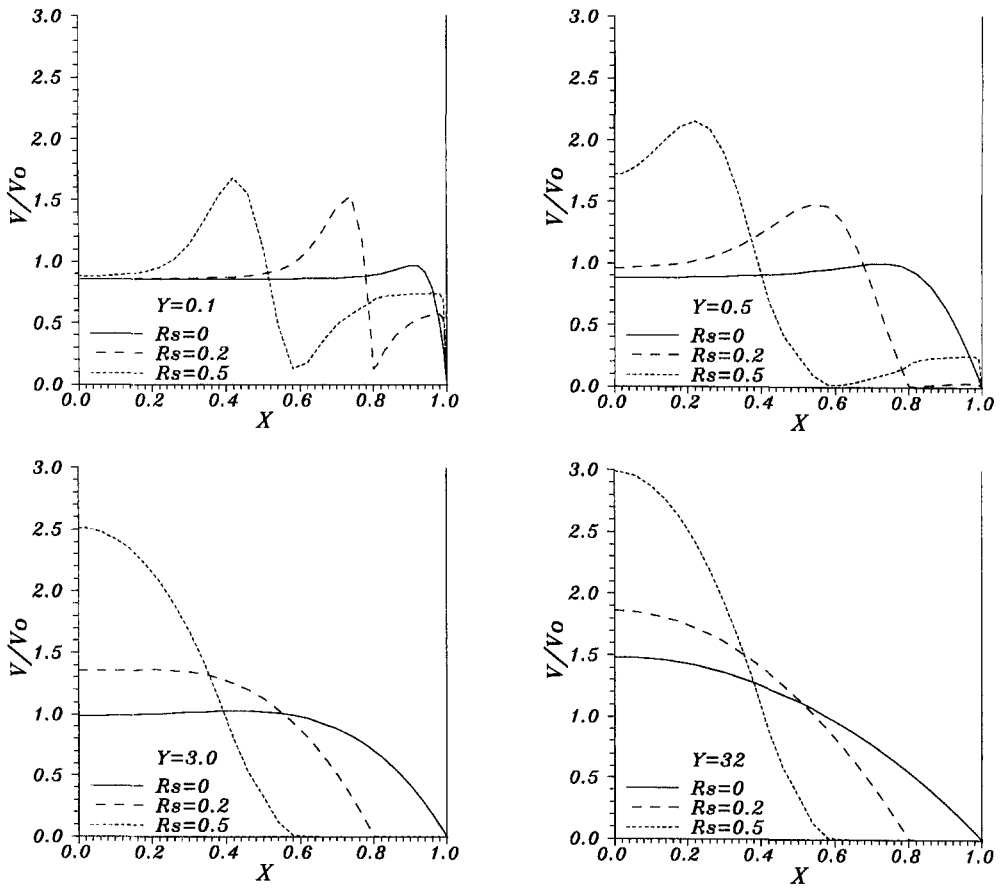

Fig. 2. The variation of velocity with different porous layer thickness ($Gr = 10^3$, $Re = 50$, $Da = 10^{-5}$, Gama = 10, $Pr = 0.72$, $\varepsilon = 0.8$).

$Rs > 0$ and at the inlet region ($Y < 0.3$), a thick porous layer inducing high fluid velocity and better convection effect results in larger local Nusselt numbers. However, as $Y > 0.3$, the Nu of $Rs = 0.2$ is greater than the Nu of $Rs = 0.5$. For $Rs = 0.5$ and at near $Y = 1$, the fluid pressure in the porous layer is a little less than the pressure in the fluid layer at the interface of composite system which results in the fluid with a lower temperature flowing into the porous layer. In the meantime, the heat transferred from the wall is less than the heat transferred out by conduction and convection in the porous medium. Hence, the bulk mean temperature T_m decreases slightly and the local Nusselt number increases slightly.

Figure 5 shows the variation of pressure drop with different porous layer thicknesses. When Rs is larger, the total drag produced by the composite parallel-plate channel is large. A greater pressure difference is

Table 2. The variation of entrance length with different parameters (general parameter values $Rs = 0.2$, $Da = 10^{-3}$, $Gr = 1000$, $Re = 50$, $Pr = 0.72$, Gama = 10, $\varepsilon = 0.8$)

Rs		*Da*		*Gr*	
parameter	length	parameter	length	parameter	length
		Hydrodynamic entrance length			
0	46	10^{-1}	46	0	7
0.2	42	10^{-3}	44	10^3	42
0.5	7	10^{-5}	42	10^4	62
		Thermal entrance length			
0	47	10^{-1}	40	0	55
0.2	55	10^{-3}	53	10^3	54
0.5	66	10^{-5}	55	10^4	49

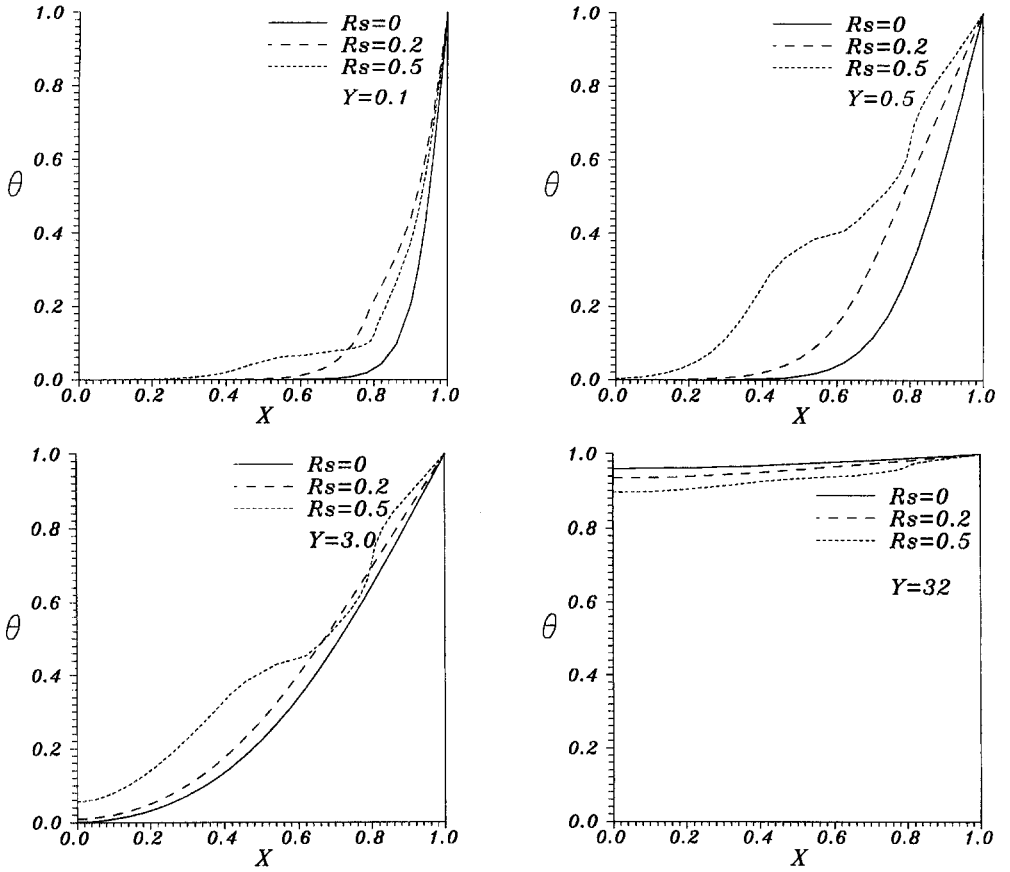

Fig. 3. The variation of temperature with different porous layer thickness ($Gr = 10^3$, $Re = 50$, $Da = 10^{-5}$, Gama = 10, $Pr = 0.72$, $\varepsilon = 0.8$).

needed to push the fluid. Figure 6 shows the variation of the local friction coefficient with different porous layer thicknesses. Due to the drag force of the porous medium, the fluid in the porous layer diminishes rapidly. This results in a great change of velocity gradient and the local friction coefficient decreases sharply at the inlet region ($Y < 2$). From the numerical results, it also can be observed that as $Y > 2$ the local friction coefficient decreases as the porous layer thickness increases from 0 to 0.2. However, the local fric-

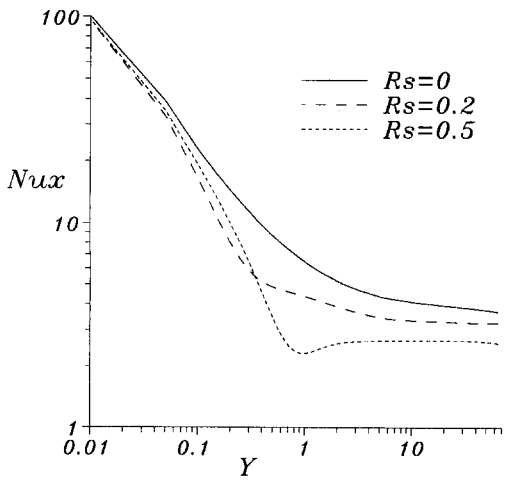

Fig. 4. The variation of local Nusselt number with different porous layer thicknesses ($Gr = 10^3$, $Re = 50$, $Da = 10^{-5}$, Gama = 10, $Pr = 0.72$, $\varepsilon = 0.8$).

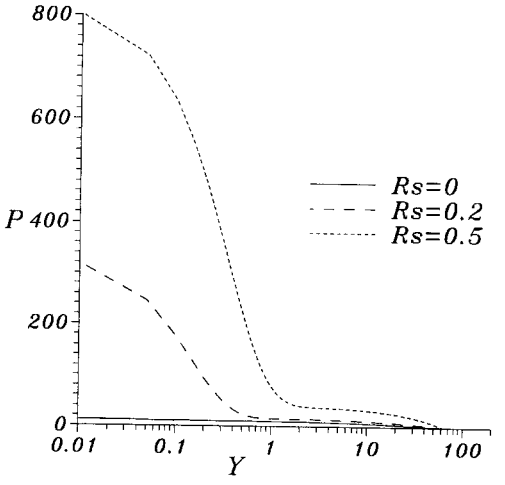

Fig. 5. The variation of pressure drop with different porous layer thicknesses ($Gr = 10^3$, $Re = 50$, $Da = 10^{-5}$, Gama = 10, $Pr = 0.72$, $\varepsilon = 0.8$).

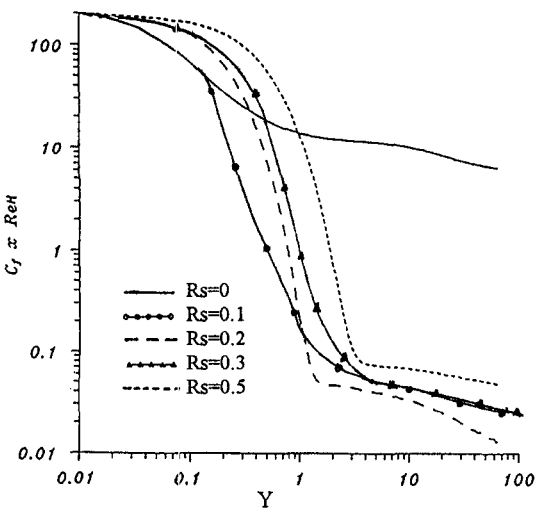

Fig. 6. The variation of local friction coefficient with different porous layer thicknesses ($Gr = 10^3$, $Re = 50$, $Da = 10^{-5}$, Gama = 10, $Pr = 0.72$, $\varepsilon = 0.8$).

tion coefficient increases as the porous layer thickness increases from 0.2 to 0.5 (due to the large velocity and velocity gradient at the wall). Therefore there is a minimum C_f existing at Rs near 0.2.

4.2. *Effects of Darcy number*

Figure 7 shows the variation of velocity with different Darcy numbers. When Y and Da are small, there is a large velocity difference at the interface of the composite system. Meanwhile, the convexity of the fluid velocity distribution in the fluid layer is obvious. When Y increases, the flow discharge in the porous layer diminishes, and the convexity of the fluid velocity profile moves to the central axis of the vertical parallel-plate channel. For small Da, i.e. low permeability, most of the fluid is forced to flow into the fluid layer, the central velocity increases, and the hydrodynamic entrance length is reduced. The results are shown in Fig. 7 and Table 2. Figure 8 shows the variation of temperature with different Darcy

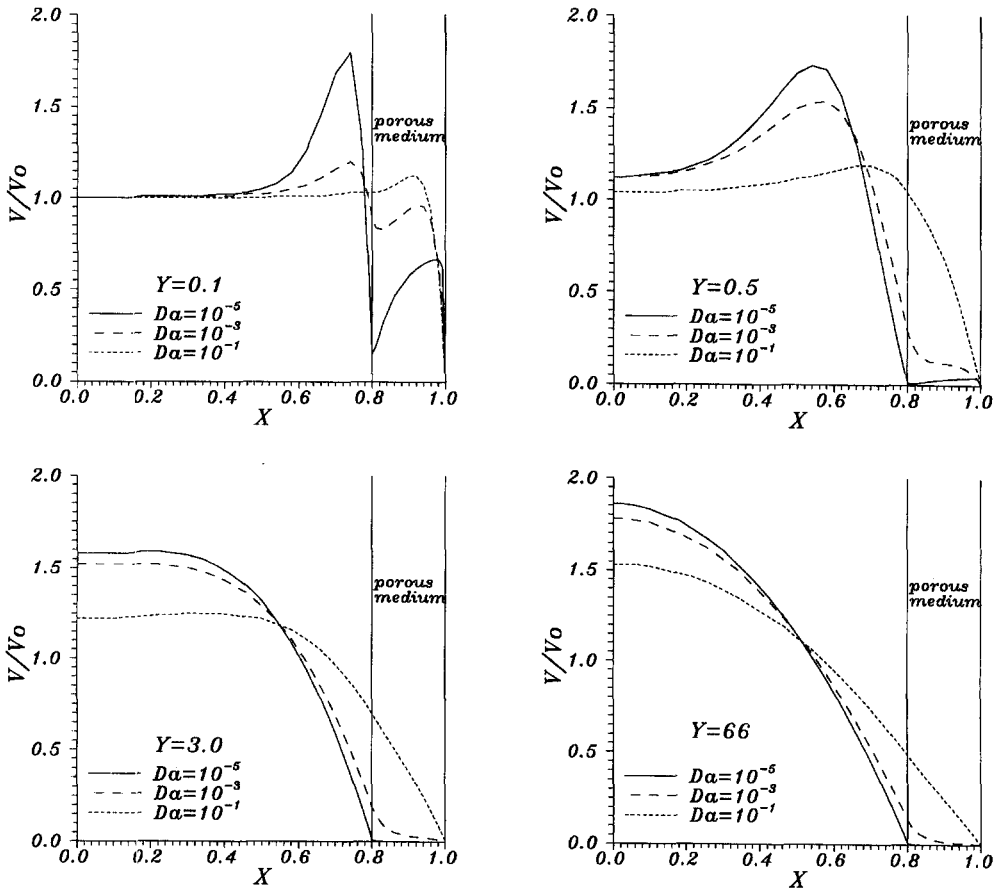

Fig. 7. The variation of velocity with different Darcy numbers ($Rs = 0.2$, $Gr = 10^3$, $Re = 50$, Gama = 10, $Pr = 0.72$, $\varepsilon = 0.8$).

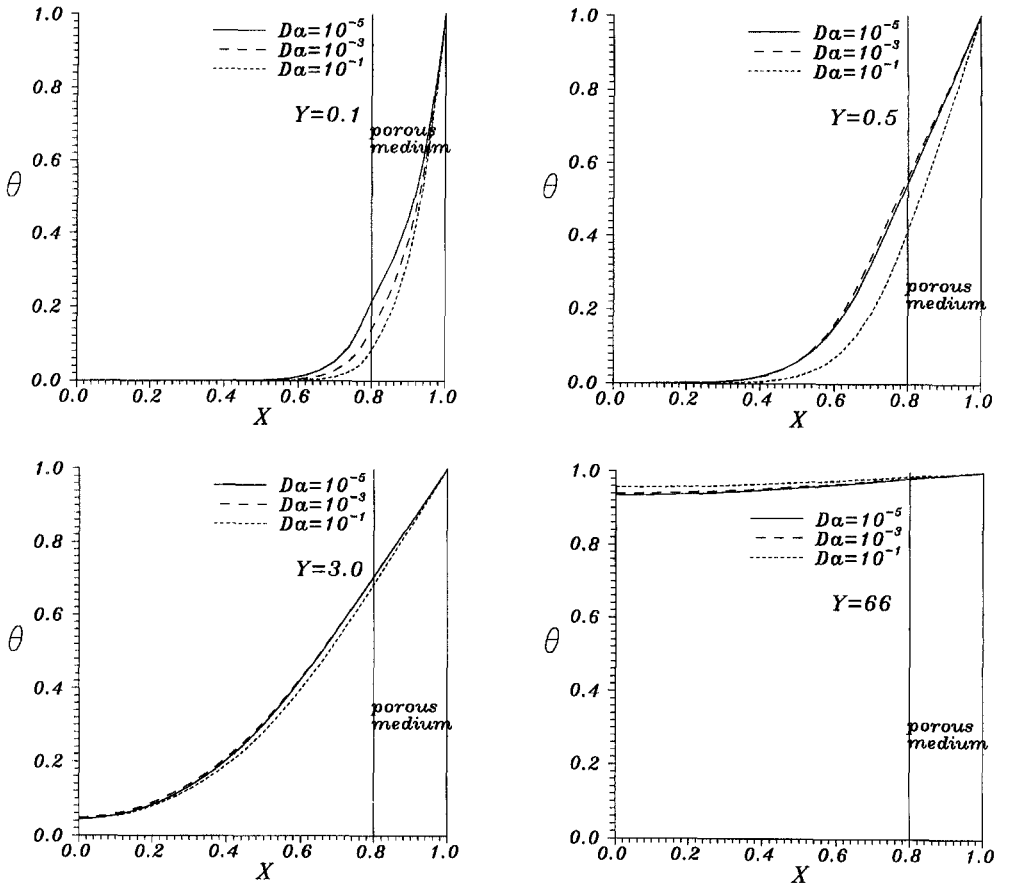

Fig. 8. The variation of temperature with different Darcy numbers ($Rs = 0.2$, $Gr = 10^3$, $Re = 50$, Gama = 10, $Pr = 0.72$, $\varepsilon = 0.8$).

numbers. At $Y < 0.5$, at the same radial position the fluid temperature is higher for the smaller Da. This is due to more heat being absorbed by the fluid in the porous layer. While Y increases, there is less fluid in the porous layer and the convective effect and temperature gradient are reduced. Therefore, the thermal entrance length increases as Da decreases. This is shown in Fig. 8 ($Y = 66$) and Table 2.

Figure 9 shows the variation of local Nusselt number with different Darcy numbers. The temperature gradient at the wall reduces as Y increases. Therefore, the heat transfer and Nu_x decreases. When Da increases, there is a larger fluid velocity in the porous layer and a larger convective effect at the wall, which increases the value of local Nusselt number. Figure 10 shows the variation of pressure drop with different Darcy numbers. When the value of Da decreases, the penetrating capability of a porous medium diminishes and induces more drag force on fluid. There is larger pressure drop existing in the entrance region, hence, the pressure drop increases as the value of Darcy number increases.

Figure 11 shows the variation of local friction coefficient at the wall with different Darcy numbers. Due to the fluid velocity, the gradient in the porous medium decreases as Y increases, the local friction coefficient decreases as Y increases. At $Y < 0.5$ a smaller Da number has a larger velocity gradient and local friction coefficient at the wall. This is due to the fact

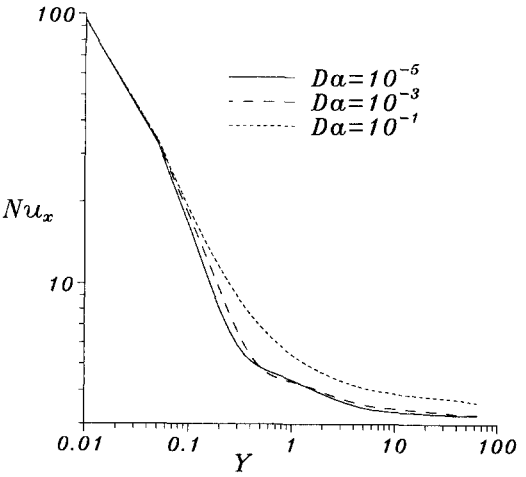

Fig. 9. The variation of local Nusselt number with different Darcy numbers ($Rs = 0.2$, $Gr = 10^3$, $Re = 50$, Gama = 10, $Pr = 0.72$, $\varepsilon = 0.8$).

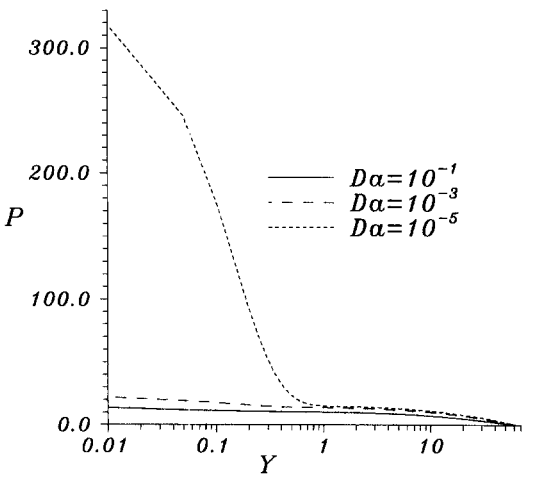

Fig. 10. The variation of pressure drop with different Darcy numbers ($Rs = 0.2$, $Gr = 10^3$, $Re = 50$, Gama = 10, $Pr = 0.72$, $\varepsilon = 0.8$).

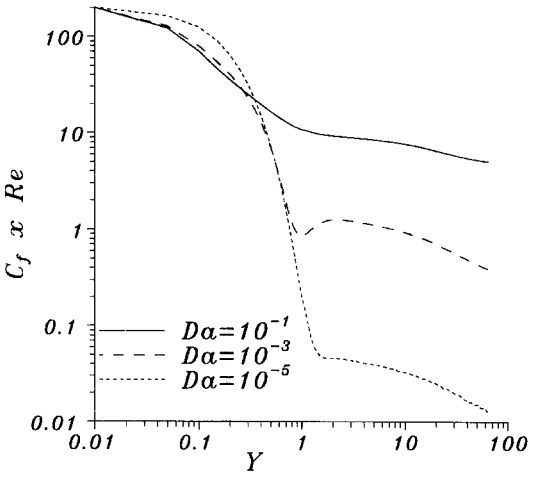

Fig. 11. The variation of local friction coefficient with different Darcy numbers ($Rs = 0.2$, $Gr = 10^3$, $Re = 50$, Gama = 10, $Pr = 0.72$, $\varepsilon = 0.8$).

that the fluid still does not flow out of the porous medium rapidly. At $Y > 0.5$, because of low flow velocity existing in the porous medium, a smaller Da has a smaller local friction coefficient.

4.3. *Effects of Grashof number*

The purpose of this section is to understand the influences of the buoyancy terms in equations (3) and (9) to the flow field and heat transfer in the composite

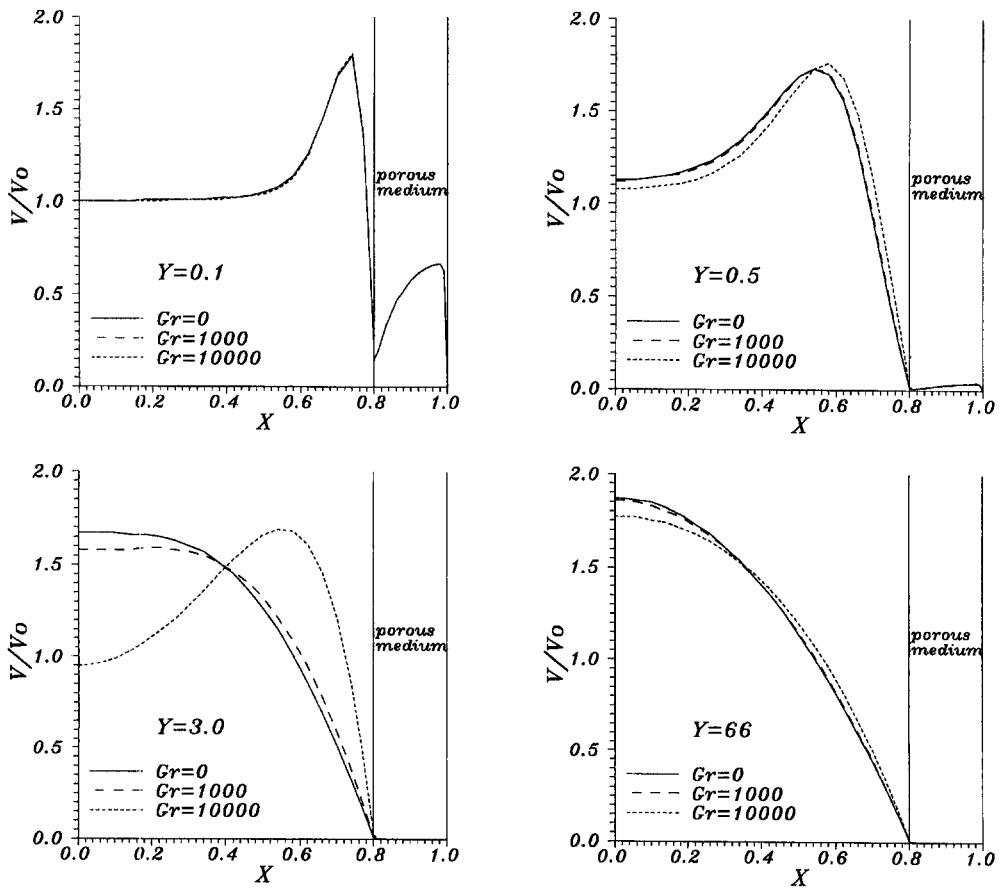

Fig. 12. The variation of velocity with different Grashof numbers ($Rs = 0.2$, $Re = 50$, $Da = 10^{-5}$, Gama = 10, $Pr = 0.72$, $\varepsilon = 0.8$).

system, i.e. the effect of Gr/Re^2. As Re is fixed, from the value of Gr/Re^2, the importance of the buoyancy terms increases with increasing Gr. Therefore, by knowing the effect of Gr, the buoyancy effect in the mixed convection of the composite system is understood.

Figure 12 shows the variation of velocity with different Grashof number. When the Grashof number increases, the fluid near the wall has a larger buoyancy force and a greater velocity. At $Y = 3.0$ and $Gr = 10^4$, the fluid near the surface of a composite system has a strong buoyancy effect which makes the central velocity smaller than the inlet velocity. When Y increases, the heat is transferred gradually into the fluid from the wall. As expected, the temperature difference and buoyancy effect of the fluid are reduced along the radial direction. For further Y position, the velocity profiles almost remain the same. From the numerical results, it is observed that the fluid velocity has only a slight difference for $Gr = 0$ and $Gr = 10^3$. For Gr greater than 1000, the buoyancy effect of the fluid has important effects. For example, the strongest buoyancy effect exists along the radial direction near $Y = 3.0$, and hence, the central velocity of the fluid is lower. When Y increases, because of the central temperature and the buoyancy effect increases, the central velocity increases. Therefore, the hydrodynamic entrance length increases as Gr increases, as shown in Table 2.

Figure 13 shows the variation of temperature with different Grashof numbers. At $Y < 0.5$, the buoyancy effect and flow velocity of fluid in a porous medium are larger for the larger Grashof number. This results a large convection and hence the fluid has lower temperature for larger Gr. At $Y = 3.0$ and $Gr = 10^4$, the fluid has a larger buoyancy effect and this makes the central velocity lower. At the same time, the fluid near the central axis absorbs more heat by conduction and has a higher temperature. Therefore, the thermal entrance length is shorter, as shown in Table 2.

Figure 14 shows the variation of local Nusselt number with different Grashof numbers. At the inlet region ($Y < 0.3$), the effect of Gr on the local Nusselt number is not obvious. When $Y > 0.3$ and $Gr > 10^3$, the convection effect produced by the buoyancy force is strong enough to increase the temperature gradient at the wall. It can be concluded that the buoyancy effect cannot be neglected when the value of Grashof number is greater than 10^4. Figure 15 shows the variation of local friction coefficient with different Grashof numbers. At $Y < 1.5$, there is a great variation of fluid velocity gradient in a porous medium,

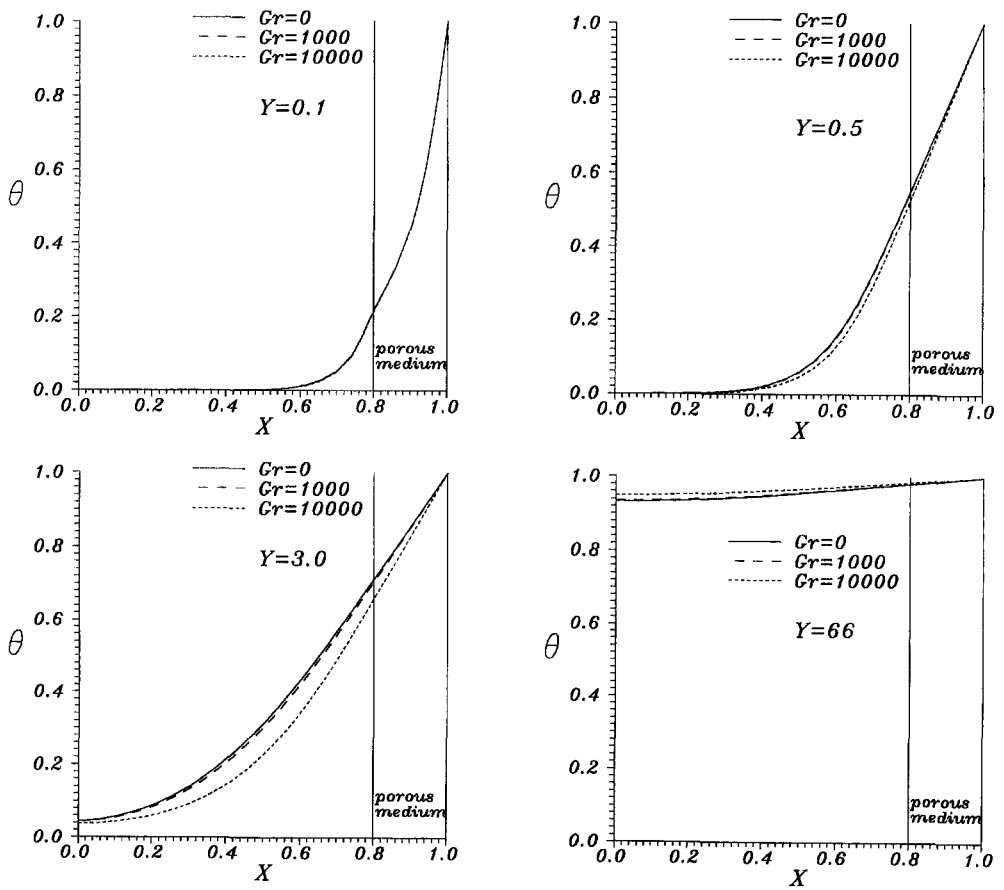

Fig. 13. The variation of temperature with different Grashof numbers ($Rs = 0.2$, $Re = 50$, Gama = 10, $Pr = 0.72$, $\varepsilon = 0.8$).

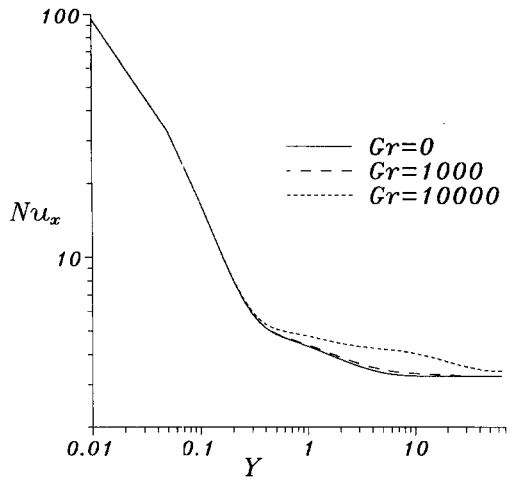

Fig. 14. The variation of local Nusselt number with different Grashof numbers ($Rs = 0.2$, $Re = 50$, $Da = 10^{-5}$, Gama = 10, $Pr = 0.72$, $\varepsilon = 0.8$).

because of this the flow discharge reduces rapidly. Hence, the local friction coefficient decreases sharply. On the other hand, at $Y > 1.5$, the local friction coefficient is very small. From the numerical results, it is found that Gr increases the fluid velocity near the wall and the local friction coefficient.

5. CONCLUSIONS

From numerical calculation and analysis, the following conclusions can be made:

(1) When a porous layer thickness increases, the local Nusselt number decreases, and pressure drop increases, the hydrodynamic entrance length becomes shorter, and the thermal entrance length becomes longer. According to the change of porous layer thickness, there is a minimum non-zero local friction coefficient existing near $Rs = 0.2$.

(2) When a Darcy number increases, the local Nusselt number and the friction coefficient increase, pressure drop decreases, the hydrodynamic entrance length becomes longer, and the thermal entrance length becomes shorter.

(3) When a Grashof number increases, the local Nusselt number and friction coefficient increase, the hydrodynamic entrance length becomes longer, and the thermal entrance length becomes shorter. Moreover, the change of velocity in the composite system is severe due to a stronger buoyancy effect.

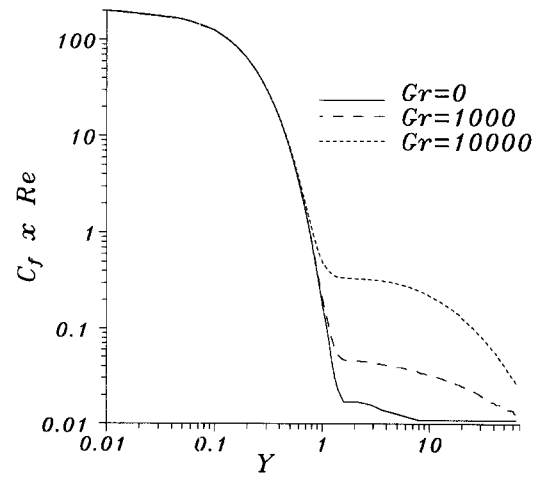

Fig. 15. The variation of local friction coefficient with different Grashof numbers ($Rs = 0.2$, $Re = 50$, $Da = 10^{-5}$, Gama = 10, $Pr = 0.72$, $\varepsilon = 0.8$).

REFERENCES

1. V. Prasad, Convective flow interaction and heat transfer between fluid and porous layers, *Proceedings of NATO Advanced Study Institute on Convective Heat and Mass Transfer in porous Medium*, Izmir, Turkey (1990).
2. D. Poulikakos, A. Bejan, B. Setmos and K. R. Blake, High Rayleigh number convection in a fluid overlaying a porous bed, *Int. J. Heat Fluid Flow* **7**, 109–116 (1986).
3. T. Schulenberg and U. Muller, Natural convection in a saturated porous layer with internal heat sources, *Int. J. Heat Mass Transfer* **27**, 677–685 (1983).
4. D. Poulikakos, Thermal instability in a horizontal fluid layer superimposed on a heat generating porous bed, *Numer. Heat Transfer* **12**, 83–89 (1987).
5. M. W. Taslim and U. Narusawa, Thermal stability of horizontally superposed porous and fluid layers, *ASME J. Heat Transfer* **111**, 357–362 (1989).
6. S. B. Sathe, L. Q. Lin and T. W. Tong, Natural convection in enclosures containing an insulation with a permeable fluid-porous interface, *Int. J. Heat Fluid Flow* **9**, 389–395 (1988).
7. C. Beckermann, R. Viskanta and S. Ramadhyani, Natural convection in vertical enclosures containing simultaneously fluid and porous layers, *J. Fluid Mech.* **186**, 257–284 (1988).
8. C. Beckermann, S. Ramadhyan and R. Viskanta, Natural convection flow and heat transfer between a fluid layer and a porous layer inside a rectangular enclosure, *ASME J. Heat Transfer* **109**, 363–370 (1987).
9. H. Campos, J. C. Morales and U. Lacia, Thermal aspect of a vertical annular enclosure divided into fluid region and a porous region, *Int. Commun. Heat Mass Transfer* **17**, 343–353 (1990).
10. K. Vafai and S. J. Kim, Analysis of surface enhancement by a porous substrate, *ASME J. Heat Transfer* **112**, 700–706 (1990).
11. P. C. Huang and K. Vafai, Flow and heat transfer control over an external surface using a porous block array arrangement, *Int. J. Heat Mass Transfer* **36**, 4019–4032 (1993).
12. G. S. Beavers and D. D. Joseph, Boundary conditions at a naturally permeable well, *J. Fluid Mech.* **30**, 197–207 (1967).
13. G. Neale and W. Nader, Practical significance of Brinkman's extension of Darcy law: complete parallel flows within a channel and a bounding porous medium, *Can. J. Chem. Engng* **52**, 475–478 (1974).
14. N. Rudraiah, Coupled parallel flow in a channel and a bounding porous medium of finite thickness, *ASME J. Heat Transfer* **107**, 322–329 (1985).
15. D. Poulikakos and M. Kazmierczal, Forced convection on a duct partially filled with a porous material, *ASME J. Heat Transfer* **109**, 653–622 (1987).
16. J. Y. Jang and J. C. Chen, Forced convection in a paralleled plate channel partially filled with a high porosity

medium, *Int. Commun. Heat Mass Transfer* **19,** 263–273 (1992).
17. K. Vafai and S. J. Kim, Fluid mechanics of the interface region between a porous medium and a fluid layer—an exact solution, *Int. J. Heat Fluid Flow* **11,** 254–256 (1990).
18. T. W. Tong and M. C. Scharatchandra, Heat transfer enhancement using porous inserts, ASME HTD 156, pp. 41–46 (1990).
19. S. Ergun, Fluid flow through packed columns, *Chem. Engng Progress* **48,** 89–94 (1952).
20. A. Bejan, *Convection Heat Transfer*. Wiley, New York (1984).
21. J. P. Van Doormaal and G. D. Raithby, Enhancements of the simple method predicting incompressible fluid flows, *Numer. Heat Transfer* **7,** 147–163 (1984).
22. S. V. Patanker and D. B. Spalding, A calculation procedure for heat, mass and momentum transfer in three-dimensional parabolic flow, *Int. J. Heat Mass Transfer* **15,** 1781–1806 (1972).
23. S. V. Patanker, *Numerical Heat Transfer and Fluids Flows*. Hemisphere, Washington (1980).